The Laryngoscope

How Design Characteristics of Tracheostomy Tubes Affect the Cannula and Tracheal Flows

Dhananjay Radhakrishnan Subramaniam, PhD; J. Paul Willging, MD; Ephraim J. Gutmark, PhD, DSc; Liran Oren, PhD

Objectives: The aim of this study was to perform computational simulations of airflow within an anatomically accurate model of an adult trachea in different tracheostomy tube designs. We hypothesized that tracheal airflow in patients is significantly influenced by the geometry and size of these devices.

Methods: The three-dimensional (3D) geometry of the trachea was reconstructed using computed tomography scans for an adult with no history of lung disease. 3D models of four cuffed tube designs, namely Tracoe, Portex, and Shiley Proximal and Distal tracheostomy tubes were generated using geometric modeling software. Transient simulations of airflow in the tube-airway assembly were performed for each tube using computational fluid dynamics (CFD).

Results: Airflow velocity was higher for the Shiley tubes compared with Portex and Tracoe tubes. For all designs, the largest magnitude of inspiratory airflow turbulence was obtained midway in the trachea. The work of breathing, quantified by the resistance of the tracheostomy tube, was lowest for Tracoe. Maximum airway wall shear stress (WSS), defined as flow-induced frictional forces, occurred at the same spatial location in all cases. Low inspiratory WSS at the carina and high expiratory airway WSS at the cuff-airway interface were observed for the Tracoe and Portex tubes.

Conclusion: Our CFD model offers a promising approach not only for choosing a tracheostomy tube for a patient but for improving existing tracheostomy tube designs.

Key Words: Tracheostomy, computational fluid dynamics, airflow characteristics.

Level of Evidence: NA.

***Laryngoscope*, 00:1–9, 2018**

INTRODUCTION

Tracheostomy is a surgical procedure that involves an incision into the trachea and placement of a prosthetic breathing device.[1] Approximately 100 thousand tracheostomy surgeries are performed every year in the United States.[2] The average length of stay in the hospital for ventilator-dependent patients with a tracheotomy is 28 days.[3] Complications after tracheostomy include bleeding, infection, pneumothorax,[4] airway stenosis resulting from granulation tissue, tracheomalacia, and airway obstruction.[5] Mortality resulting from vascular injury has also been reported in a small number of patients.[6]

In vitro studies have been performed to study the airflow characteristics of endotracheal[7,8] and tracheostomy[9–12] tubes. in vivo studies have also been performed to study the airflow characteristics for tracheostomy[13] and endotracheal tubes[8] following intubation. These studies quantified the effectiveness of the tube design by evaluating the work of breathing[13] and compared the work of breathing for different tube designs. Experimental studies indicated that over- or underinsertion of tracheostomy tubes into the airway can increase airway resistance.[10] Differences in airflow among the various tube designs have been described as important factors in the selection of the tracheostomy tube for patients requiring ventilator-assisted breathing.[11]

Advances in computational fluid dynamics (CFD) have enabled simulations of airflow in rigid[14,15] and compliant models[16] of anatomically accurate healthy and diseased tracheas. The effect of various airway surgeries performed to correct obstructive sleep apnea, expressed as a change in the work of breathing, were evaluated preoperatively using CFD modeling.[17,18] CFD modeling has also been effective in estimating three-dimensional variations in flow-induced frictional stresses,[19] which are hypothesized to influence the inflammation of soft and cartilaginous tissue through the trauma induced by the flow of air against the tissue.[20] Spatial variation in airflow turbulence, determined as a function of the inner cannula diameter,[21] can be evaluated more accurately than in vitro or in vivo studies using CFD.[22]

From the Department of Aerospace Engineering and Engineering Mechanics, University of Cincinnati (D.R.S., E.J.G.); the Department of Otolaryngology–Head and Neck Surgery, University of Cincinnati College of Medicine (J.P.W., L.O.); and the Division of Pediatric Otolaryngology, Cincinnati Children's Hospital Medical Center (J.P.W.), Cincinnati, Ohio, U.S.A.

Editor's Note: This Manuscript was accepted for publication on August 16, 2018.

Presented at the Combined Otolaryngology Spring Meeting, National Harbor, Maryland, U.S.A., April 20–21, 2018.

Support for this project was through an unrestricted educational grant to the University of Cincinnati from Bryan Medical. The authors have no other funding, financial relationships, or conflicts of interest to disclose.

Send correspondence to Liran Oren, PhD, Department of Otolaryngology–Head and Neck Surgery, University of Cincinnati College of Medicine, PO Box 670528, Cincinnati, OH 45267. E-mail: orenl@ucmail.uc.edu

DOI: 10.1002/lary.27569

In this study, we hypothesized that specific design characteristics of tracheostomy tubes can alter the characteristics of airflow through the cannula and the tracheal airway. Defining how the tube's design affects cannula and tracheal flow is important to further understand potential mechanisms that may increase the resistance to breathing and prolong the weaning process from a ventilator. Potential conditions that may induce tissue irritation due to the shear forces of the airflow impinging the airway mucosa may also be predicted.

MATERIALS AND METHODS

Airway Model Construction and Tracheostomy Tube Geometries

In this study, computed tomography (CT) scans from a healthy 43-year-old subject with no history of lung disease were used to construct the mathematical trachea model. Images obtained from a public repository (www.osirix-viewer.com) were acquired during peak exhalation using a 16-detector CT scanner. The scans consisted of 200 slices (each 2 mm thick) extending from the thyroid cartilage to the tertiary bronchi (Fig. 1a). The spatial resolution of the images was 512 × 512 pixels (pixel spacing 0.7422 × 0.7422 mm). Construction of the model's geometry of the trachea (Fig. 1b) was done using commercially available software (Mimics Research, Materialise NV, Leuven, Belgium). The four tracheostomy tubes tested included Tracoe twist plus size 9 (TRACOE medical GmbH, Nieder-Olm, Germany), Portex cuffed DIC size 9 (Smiths-Medical, Minneapolis, MN), and proximal and distal versions of the Shiley XLT size 7 tubes: Shiley P and Shiley D, respectively (Medtronic, Minneapolis, MN). Outer cannula diameters were 12.1 mm for Tracoe, 12.6 mm for Portex, and 12.3 mm for both the Shiley tubes. Their inner cannula diameters were 9, 8, and 7 mm, respectively. The inner and outer cannula diameters were provided by the manufacturers. Lengths of the inner cannula were 79, 90, and 100 mm for the Portex (Smiths-Medical), Tracoe (TRACOE medical GmbH), and both Shiley (Medtronic) tubes, respectively. The proximal, radial, and distal lengths for Shiley P were 27, 39, and 34 mm, respectively. The corresponding lengths for Shiley D were 12, 39, and 49 mm, respectively. The exact geometry of each tube was reconstructed from micro-CT scans (Fig. 1c) to best capture its geometrical details (e.g., corrugation of the inner cannula of the Shiley tubes) (Fig. 1d).

Airway–Tracheostomy Tube Assembly and Simulations of the Respiratory Cycle

For consistency, the computational domains for the models were generated such that each tracheotomy tube was aligned with the trachea's centerline. The tracheotomy tube cuff was sealed to the tracheal wall in the virtual model to ensure that airflow did not leak into the upper respiratory tract (Fig. 1–2).

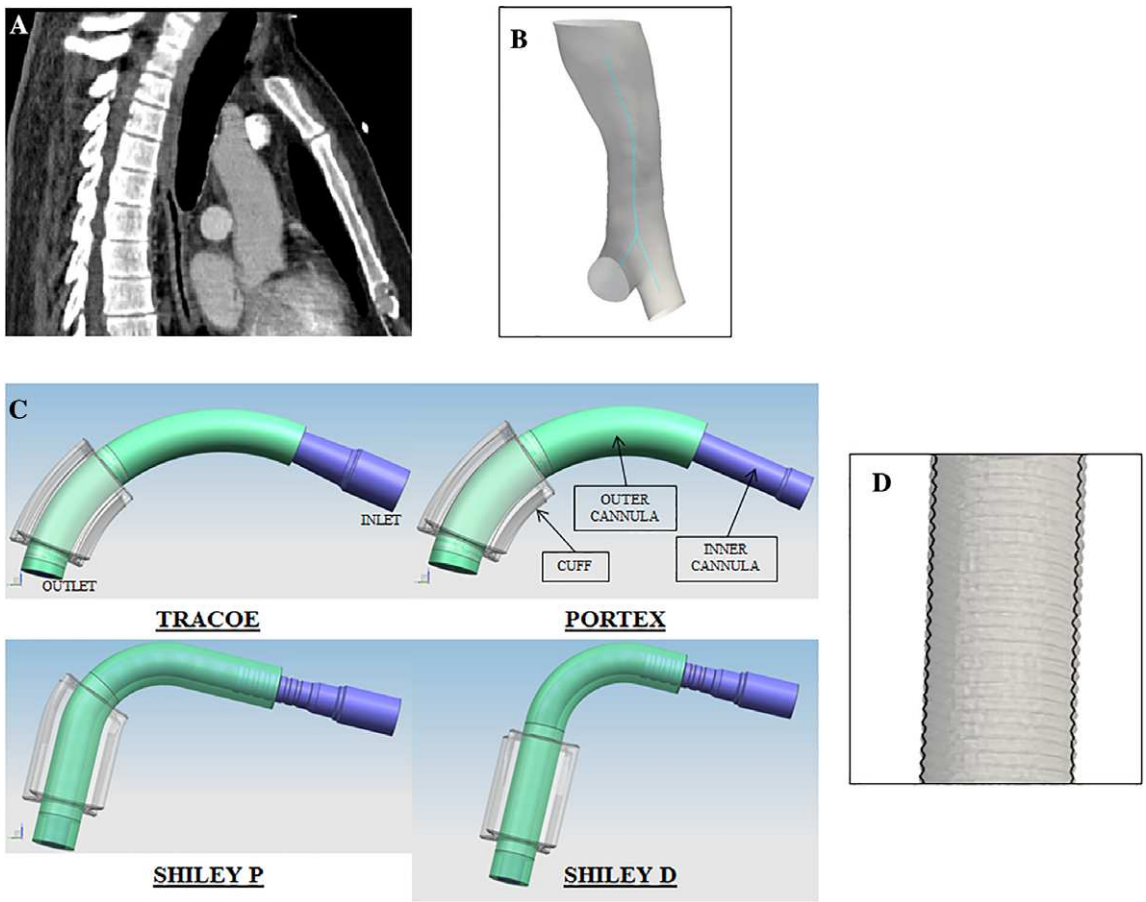

Fig. 1. (a) Sagittal computed tomography image used to reconstruct the airway model. (b) Reconstructed 3D airway model (blue line: trachea's centerline). (c) Reconstructed geometries of the four tracheostomy tubes. (Outside diameters of the tracheostomy tubes ranged from 12–13 mm in this study). (d) Saw-tooth profile corresponding to Shiley tubes.

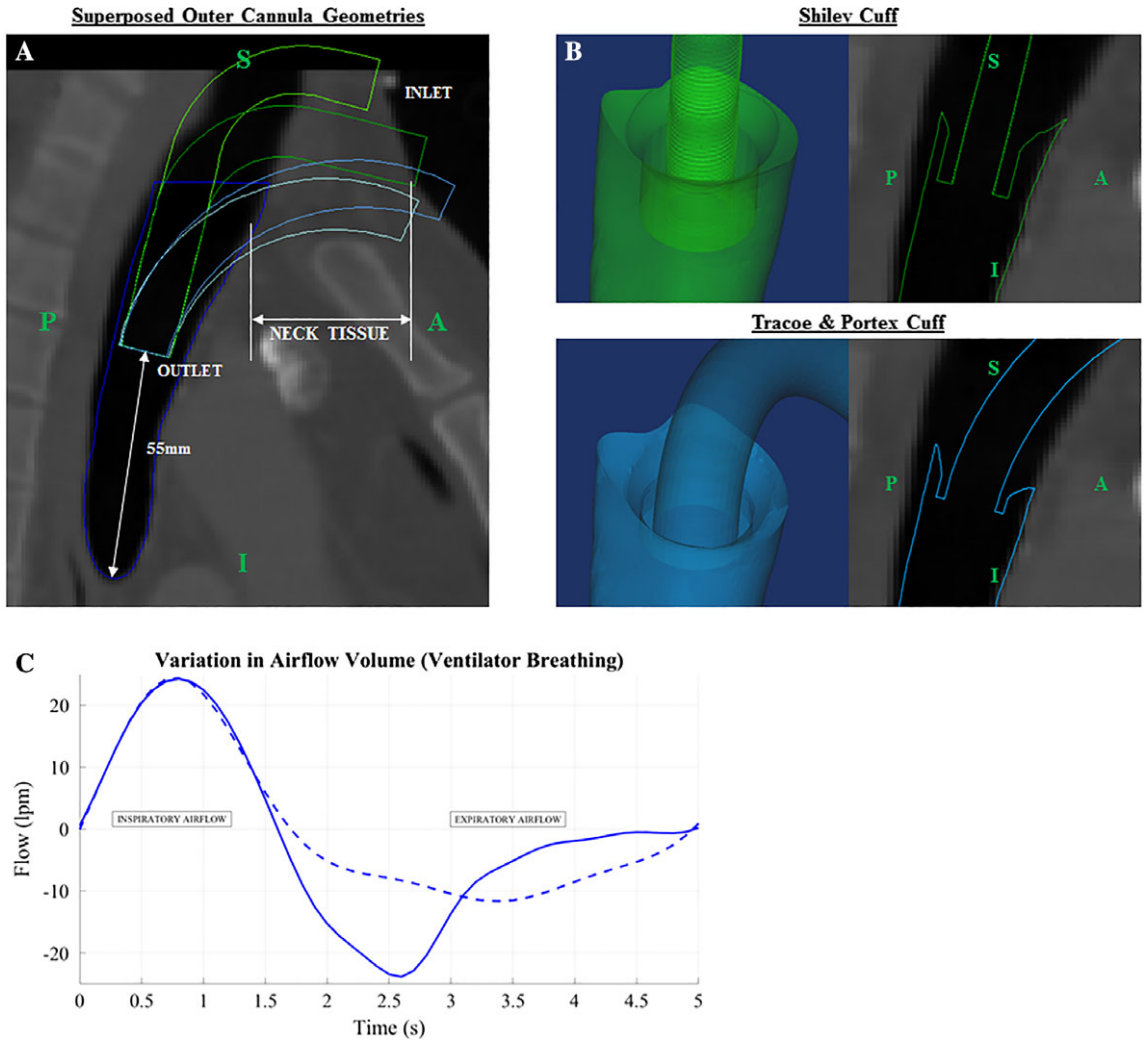

Fig. 2. (a) Schematics of the tube placement within the airway. Outer cannula shown for reference, Tracoe (blue), Portex (light blue), Shiley D (light green), and Shiley P (dark green). (b) Representation of the configuration of the inferior aspect of the tracheotomy tube cuff and its interface with the trachea. (c) Airflow profiles for natural (dashed blue line) and ventilator-assisted breathing (solid blue line).

To ensure an optimal comparison of flow characteristics, the distal end of every cannula was set to 55 mm above the carina (Fig. 2a). As a result of aligning the distal end of the tracheotomy tubes at this fixed point and ensuring that the midline of the tube was in the center of the trachea, the location of the tracheotomy tube flange varied in its location in the neck due to the variations in tube curvature and overall length of the tracheotomy tube. The fact that some of these tubes were theoretically located within the neck tissues of the model patient used in this study did not affect the simulations. That is, the volume of the computational airflow domain consisted of the inner cannula and airway lumen downstream of the distal end of the tracheotomy tube (Fig. 2b). Simulations of airflow were performed using input conditions of natural and ventilator-assisted breathing (Fig. 2c).[23,24] The inhalation flow profile was assumed to be identical for these two cases, and a phase shift corresponding to peak exhalation was obtained for ventilator breathing.

Airflow dynamics in the models were predicted using a commercially available CFD solver (ANSYS Fluent, ANSYS Inc., Pittsburgh, PA) with Unsteady Reynolds-Averaged Navier Stokes simulations. A tetrahedral mesh[25] corresponding to 3 million elements for Portex and Tracoe and 6.5 million elements for Shiley airway-tube geometries were generated using ANSYS T-Grid (ANSYS Fluent). The tetrahedral cells were combined into polyhedral elements to ensure homogenous distribution of wall quantities.[26] A k-ω SST turbulence model,[17] turbulence intensity of 5%, and a length scale of 0.5 mm was assumed for all cases. A velocity boundary condition was prescribed at the tracheostomy tube inlet, and static pressure outlet boundary conditions were specified at the tracheal bifurcation.[27] An implicit time-integration scheme[27] and 1 hundred time steps per respiratory cycle were employed in the study. The spatial and temporal discretization was of the same order of magnitude employed in a previous study.[27]

RESULTS

Changes in Flow Due to Differences in the Inner Wall Diameter of the Tracheotomy Tube

Flow velocity and turbulence were characteristics most affected by the variations in the inner diameter of the cannula. Flow velocities were highest for the Shiley

tubes (Medtronic) due to their smaller inner cannula diameter among those analyzed in this study (Fig. 3). The prediction of higher velocity for smaller diameters, which follows the Bernoulli principle, was observed throughout the respiratory cycle. These higher flow velocities were also computed in the trachea for the two Shiley tubes (Medtronic). Regardless of the tracheotomy tube tested, the CFD simulations showed the inspiratory airflow to exit the cannula as a jet, which then impacted against the carina of the trachea.

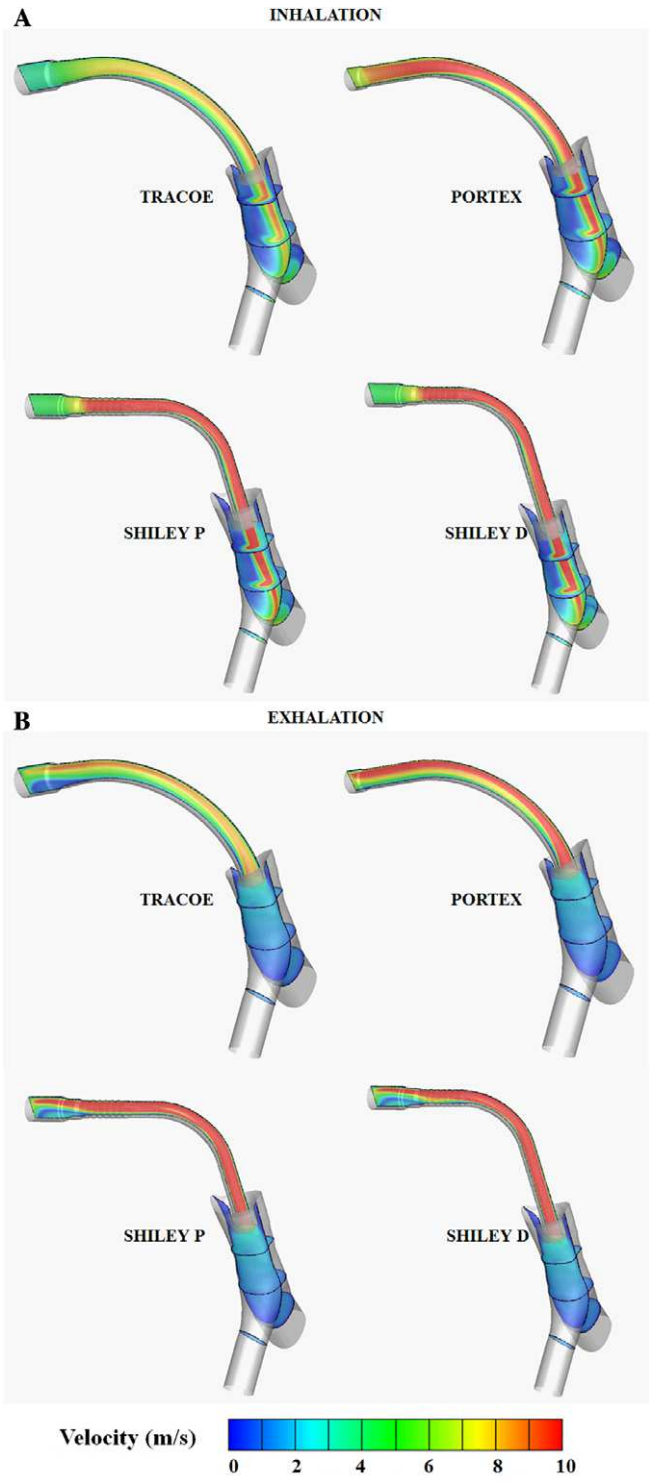

Fig. 3. Contours of velocity magnitude showing flow patterns for ventilator-assisted breathing during (a) peak inhalation and (b) peak exhalation.

The temporal changes in turbulence (quantified using the turbulent kinetic energy) were shown for a location midway between the lower end of the tracheotomy tube and the carina (30 mm above the carina) (Fig. 4a) and in the inlet of the tracheostomy tubes (Fig. 4b). Turbulence in the trachea was highest during peak inspiratory flow for all tubes. The phase of the peak inspiratory turbulence in the trachea was unchanged for ventilator breathing because the inspiratory flow conditions were identical for natural and ventilator breathing. However, the turbulence predicted in the trachea during inspiration was 100% greater for the two Shiley tubes (Medtronic) than that found in the Tracoe (TRACOE medical GmbH) or Portex (Smiths-Medical) tubes.

During exhalation, the simulations predicted marked differences at the inlet for the different tubes (Fig. 4b). The peak expiratory turbulence at the inlet was predicted to be four times higher for both the Shiley (Medtronic) tubes under normal breathing conditions and was also four times higher for ventilator-assisted breathing conditions. The phase where the peak expiratory turbulence occurred matched the peak phase of the exhalation flow (c.f., Fig. 2c). Differences in turbulence level between inspiratory and expiratory flow conditions directly related to higher flow velocities associated with the Shiley tubes (Medtronic).

Marked differences were also observed in the spatial distribution of turbulence along the tube-airway assembly (Fig. 5). During peak inhalation, turbulence was stable throughout the tubes, followed by an increase in the trachea, which stemmed from the jet-like behavior of the flow (Fig. 5a). The sudden expansion of the flow from the cannula into the trachea induced instabilities due to the difference in regions with high momentum (i.e., fast moving) and stagnant flows. Similar behavior in spatial variation was observed for peak exhalation (Fig. 5b), but with notable differences between natural and ventilator-assisted breathing conditions.

Changes in Flow Due to Difference in Curvature of the Tracheotomy Tubes

Wall shear stress (WSS), which is defined as the gradient of flow velocity, represents the frictional stresses on the surface of the airway. WSS was used to assess how different tube curvatures affected airflow. The nearly uniform distribution of WSS values computed for the Tracoe (TRACOE medical GmbH) and Portex (Smiths-Medical) tubes stemmed from their gradual change in curvature and indicates that the flow remained attached to the inner wall (Fig. 6). The figure shows the WSS distribution for (peak) inhalation. The distribution of expiratory WSS was qualitatively similar. The higher flow velocities in the Portex tube lead to the greater magnitude of WSS. In contrast, the variable WSS values (low/high values) computed for the Shiley tubes (Medtronic) were indicative that the flow separated from the inner wall of the cannula due to the corrugated configuration of the inner cannula.

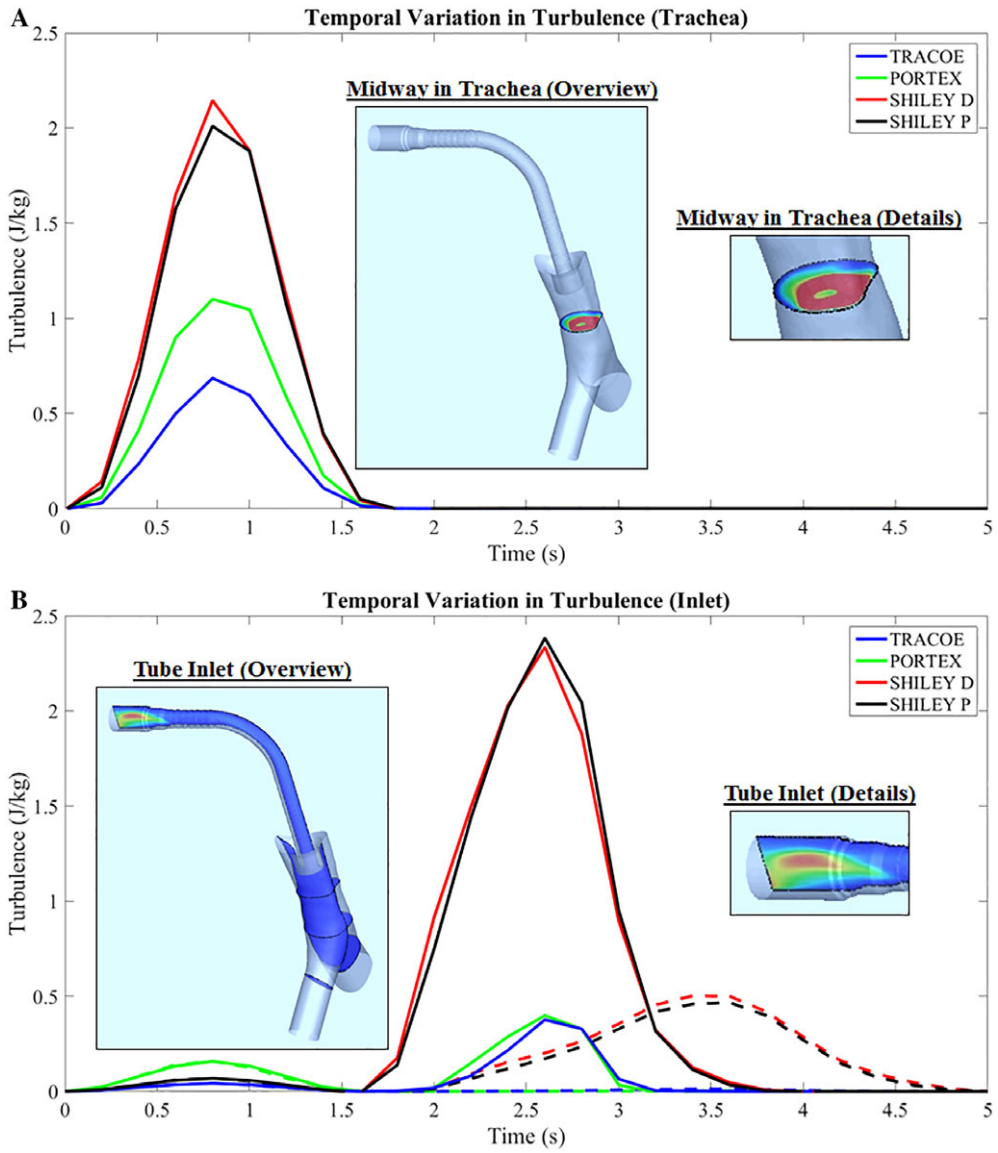

Fig. 4. Temporal variation in turbulence in the (a) trachea and (b) inlet. Dashed lines correspond to natural breathing. Inset contour plots show the instantaneous turbulence distribution during its peak moment.

The highest WSS values for the Shiley tubes were computed at the 90° bend of the cannula. The lower WSS values for these tubes were computed for regions upstream and downstream from the bend. The flow separation in the Shiley tubes also indicated that the corrugation profile of the cannula did not affect the flow profile. The WSS distribution during inspiration was identical for natural and ventilator-assisted breathing.

The jet of air that exited the distal end of the tracheostomy tube during inspiration impinged on the carina and created regions of high WSS at this site (Fig. 7a). Inspiratory WSS at the tracheal bifurcation was greatest for the Shiley P (3.3Pa) (Medtronic) and least for the Tracoe (TRACOE medical GmbH) tube (1.9Pa) due to lower airflow velocity for the latter. During peak exhalation, the magnitude and location of maximum WSS (midway in the trachea) was identical for all cases (Fig. 7b, black arrows). The magnitude of WSS for natural breathing was 25 times lower during expiration than inspiration. During exhalation, a second region of high WSS was observed in the area of the cuff-airway interface (Fig. 7b). In this region, WSS values were significantly lower for the Shiley (Medtronic) tubes, probably because the geometry of the inflated Shiley cuff created a stagnant zone of air where the cuff contacted the tracheal wall. This observation, however, should be interpreted cautiously because we could not verify the accuracy of the shape of the virtually inflated cuff.

Difference in Airflow Resistance

The work of breathing was assessed by comparing the flow resistance for each tube. Flow resistance was defined as the ratio of the pressure drop (i.e., difference

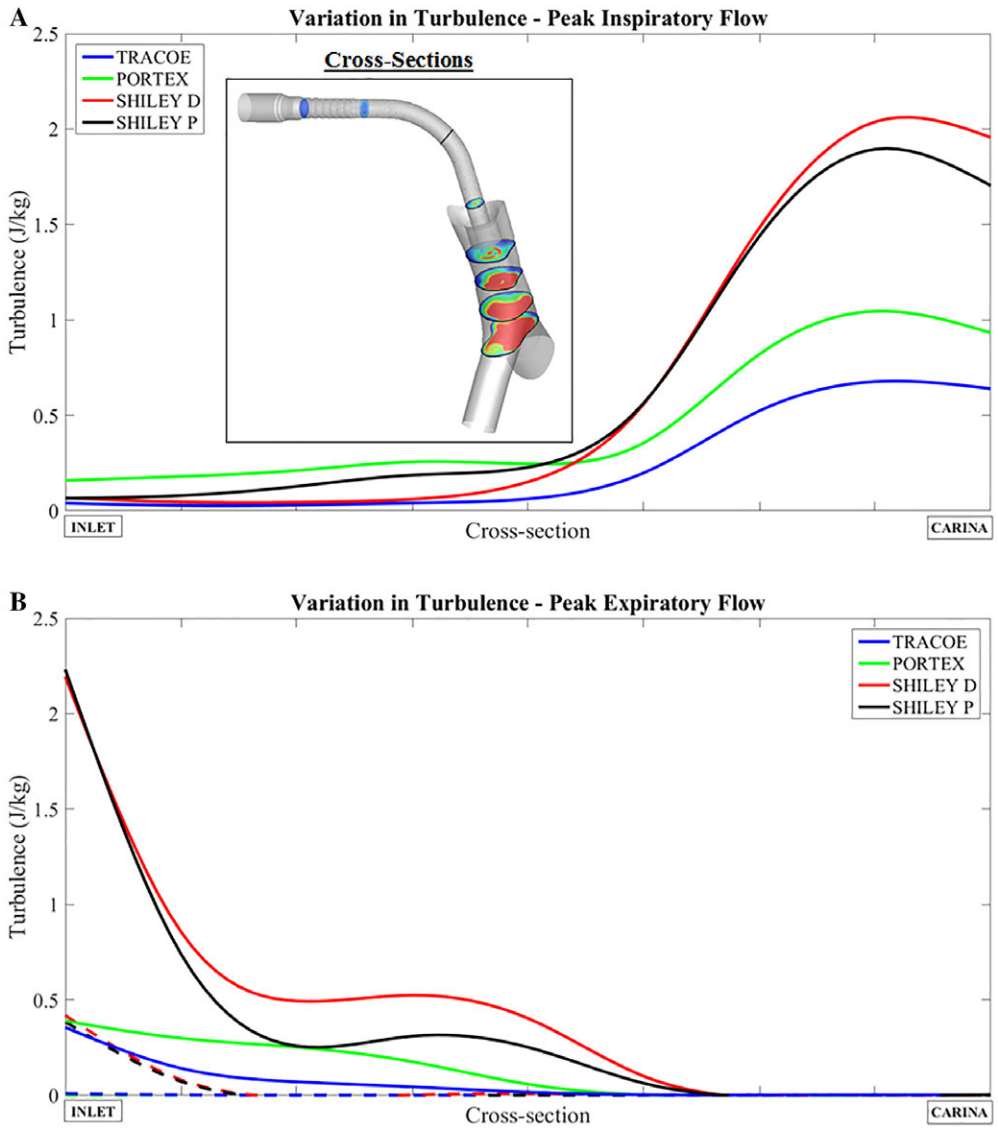

Fig. 5. Spatial variation in turbulence along the tube-airway assembly during (a) peak inspiration and (b) peak expiration. Markers are the same as in Figure 4. Inset shows cross-sectional planes sampled along the airway-tube assembly.

between pressures at the inlet and outlet) to the flow rate during inhalation or exhalation: $R = \Delta P / Q_{peak}$. The simulations showed that peak inhalation resistance was similar between the two Shiley (Medtronic) tubes; however, the values were 175% higher than that calculated for the Tracoe (TRACOE medical GmbH) tube and 125% higher than the Portex (Smiths-Medical) tube (Fig. 8a). Inhalation resistance was identical for natural and ventilator breathing because there was no difference in the flow rates. Compared with inhalation, the flow resistance values were an order of magnitude lower for peak exhalation, corresponding to ventilator-assisted breathing (Fig. 8b). The difference in peak exhalation flow rate also explains why the resistance for ventilator breathing was higher for all the tubes compared to natural breathing. Exhalation resistance was predicted highest for the Portex tube. The resistance for the two Shiley (Medtronic) tubes was comparable to values calculated for Portex (Smiths-Medical) for both natural and ventilator breathing conditions. The higher expiratory resistance for the Portex tube might stem from the slightly thicker boundary layer (i.e., yellow and green sections) on its curved section (Fig. 3b), which reduces its effective diameter and therefore makes the resistance during exhalation more comparable with the Shiley (Medtronic) tubes. The Tracoe (TRACOE medical GmbH) tube resistance was 60% lower than the Portex (Smiths-Medical). These flow resistance results suggest that the overall work of breathing is higher for the Portex and Shiley tubes, when compared to Tracoe.

DISCUSSION

In testing four tracheostomy tube designs in simulations of natural and ventilator-assisted breathing, our findings confirmed our hypothesis that certain geometric design characteristics lowered airflow resistance and

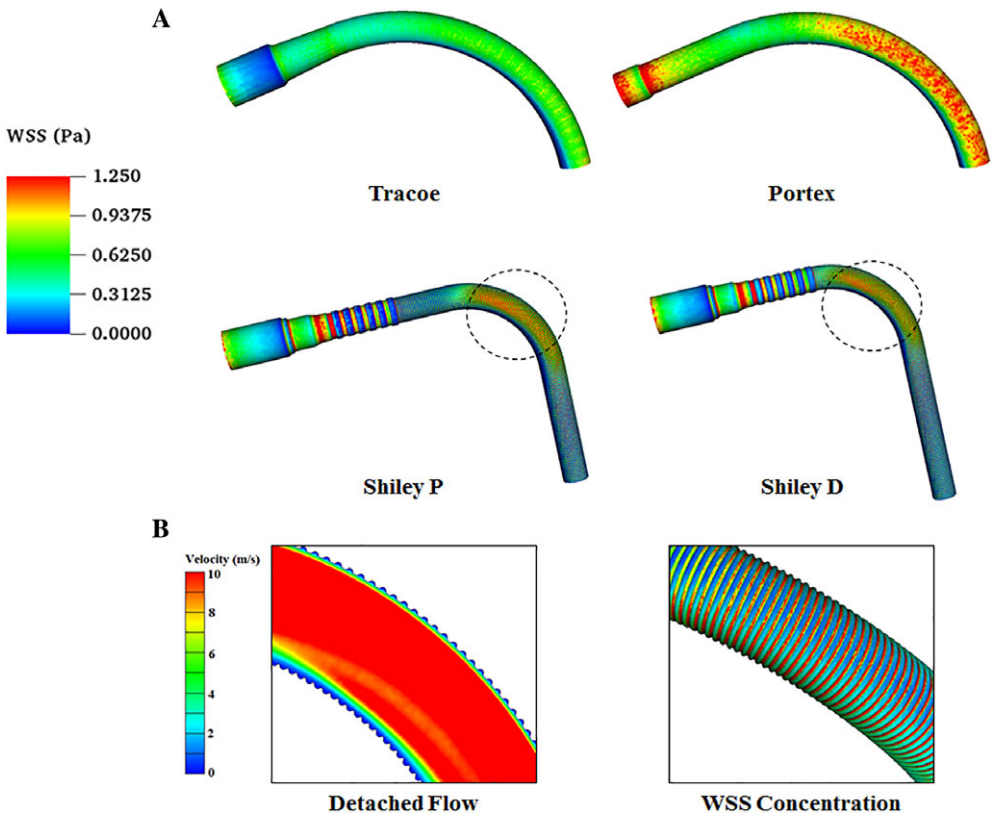

Fig. 6. (a) Comparison of tracheostomy tube WSS for peak inspiratory flow (sagittal views indicated for all tubes). (b) Details of detached flow at the 90° bend of the Shiley tubes. WSS contour shown on the right, and velocity contour shown on the left.WSS = wall shear stress.

reduced aerodynamic forces. In our model of tracheotomy tubes with relatively similar outer diameters, the smaller inner diameter Shiley (Medtronic) tubes yielded higher flow velocities than the Tracoe (TRACOE) and Portex (Smiths-Medical) when using the same flow rate. This observation is in agreement with findings from previous studies.[12,13] The smaller diameters combined with the sharper bending and nonuniform tube surface morphology of the Shiley (Medtronic) tubes were likely responsible for the higher turbulence levels. Our findings were also in good agreement with previous experimental studies that demonstrated lower airway resistance in Portex (Smiths-Medical) and Jackson tubes with a smooth inner cannula surface as compared to Shiley (Medtronic) tubes with a saw-tooth surface profile.[12]

Our simulations showed that, during inhalation, the tracheal airflow impinged on the carina and created a region of high WSS (more so for the Shiley tubes). During exhalation, a region of high velocity and shear stress was formed superior to the bifurcation in the trachea due to merging of the flow from the mainstem bronchi. With these current observations in agreement with previous studies,[19,28] clinicians should consider the effect of WSS within the lower trachea and at the carina that may cause impingement of the tracheal flow on the cartilage or airway mucosa, which can potentially lead to tissue inflammation and injury. Previous experimental studies involving tracheal epithelium tissue cultures from Fischer 344 rats exposed to transmembrane pressures showed the induction of early growth response-1 (Egr-1), endothelin-1, and transforming growth factor-B1.[29] This demonstrates that mechanical forces may play a role in tissue remodeling and cellular homeostasis. WSS may induce cellular changes of inflammation, which stimulate fibroblast proliferation and collagen production.[29] In addition, airflow turbulence has been previously described to generate high WSS and disrupt the healing process of inflamed tracheal smooth muscle, previously injured by an infection.[25] Clinically, granulation tends to occur in areas that correlate with increased WSS, such as the end of a tracheotomy tube and at the carina. Minimizing airflow-induced trauma may minimize the development of granulation tissue within the airway.

Our results also showed that the junction between the cuff and the tracheal wall that formed when the cuff was inflated is another region where higher WSS occurs during the exhalation phase. Tissue inflammation as a result of the pressure exerted by the cuff on the airway wall has been suggested previously,[30] but our findings can be used to develop a more robust model to describe the biomechanical interaction between the inflated cuff and airway wall.

Study Limitations

The main limitation of our study was the lack of postoperative CT scans to validate the alignment of the

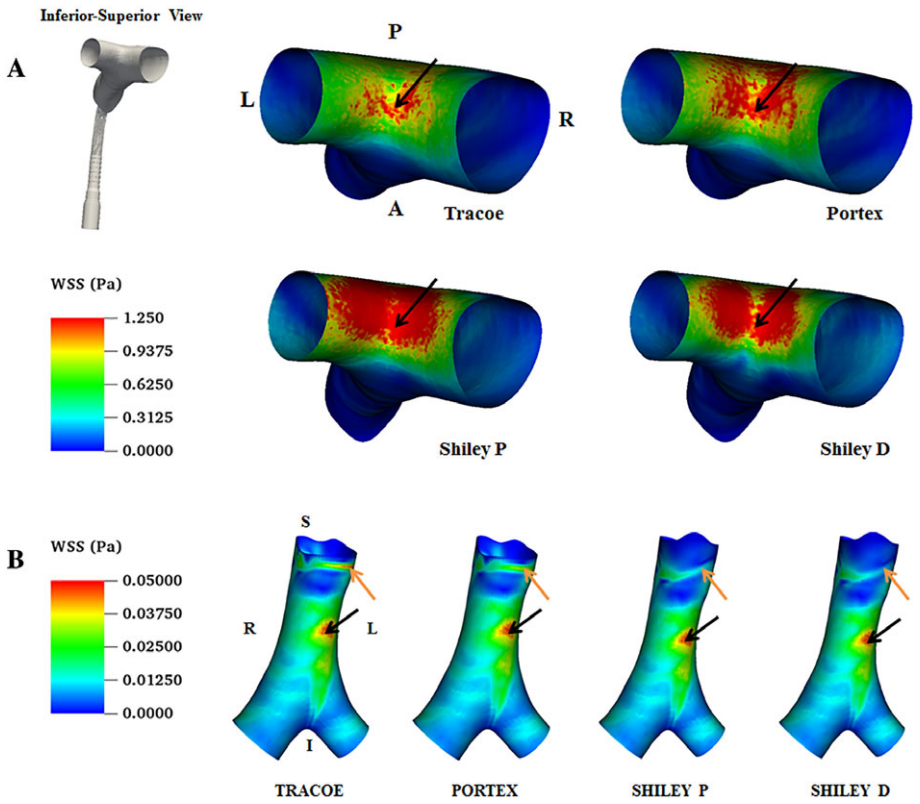

Fig. 7. Comparison of airway WSS (a) peak inspiratory views shown in the I–S direction. Black arrows indicate location of highest shear stress. Distribution is identical for natural and ventilator breathing. (b) Peak expiratory airway WSS views shown in the A–P direction. Black and orange arrows mark the location of highest airway WSS location in the airway and cuff-airway interface, respectively. Note that WSS values for inspiration/expiration are shown on a different scale.A = anterior; I = inferior; L = left; P = posterior; R = right; S = superior; WSS = wall shear stress.

tracheostomy tubes and the inflated shape of the cuff. We also considered only one possible (input) waveform for both the natural and ventilated breathing conditions. Other flow waveforms are likely to yield flow behaviors that quantitatively differ but are qualitatively similar to our findings. Finally, our study did not consider how changing the distance between the carina and distal end of the tracheotomy tube would affect our results.

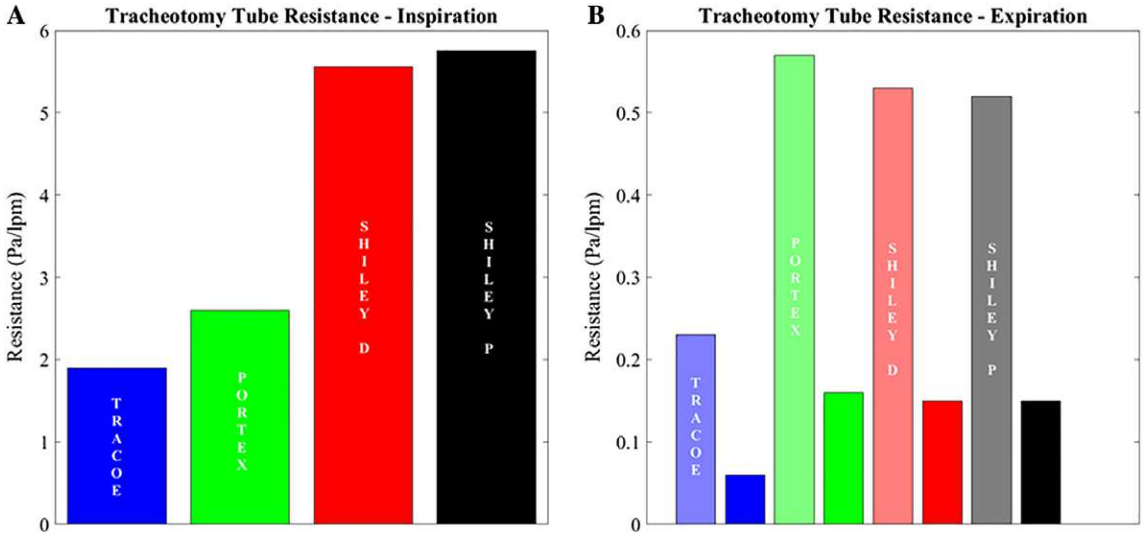

Fig. 8. Comparison of airflow resistance: (a) Inspiratory resistance, and (b) expiratory resistance. Transparent bars correspond to ventilator breathing. Note that resistance values for inspiration/expiration are shown on a different scale.

Future Directions

Previous studies have emphasized the need to individualize or customize the tracheostomy procedure and use tubes based on a patient's clinical[31] and anatomical[32] characteristics. The different geometry of various manufacturers of tracheotomy tubes allow a surgeon to select the cannula that best conforms to an individual patient's anatomy. The basic design characteristics of the cannula may have effects on the ease of ventilation of the patient and possibly affect the ease with which a patient may be weaned from a ventilator and eventually decannulated.[28] We suggest that there can be an ideal tracheotomy tube design that combines the advantages of curved and angled tubes with a maximum inner cannula diameter.

CONCLUSION

Our study analyzed flow patterns, turbulence, WSS, and airflow resistance for four tracheostomy tube designs of similar outer diameter. Flow velocity and turbulence were highest for the Shiley (Medtronic) tubes due to the smaller inner cannula diameter. The spatial location of maximum airway turbulence and WSS was similar for all tubes. The Portex (Smiths-Medical) and Tracoe (TRACOE medical GmbH) tubes exhibited lower airway resistance and airway WSS compared with the Shiley (Medtronic) tubes, at least for the conditions employed in this pilot study. Our findings could potentially assist clinicians in evaluating the effectiveness of a tracheostomy tube, with respect to its airflow characteristics.

BIBLIOGRAPHY

1. Susanto I. Comparing percutaneous tracheostomy with open surgical tracheostomy: both will coexist until robust evidence becomes available. *BMJ* 2002;324:3–4.
2. Yu M. Tracheostomy patients on the ward: multiple benefits from a multidisciplinary team? *Crit Care* 2010;14:109.
3. Engoren M, Arslanian-Engoren C, Fenn-Buderer N. Hospital and long-term outcome after tracheostomy for respiratory failure. *Chest* 2004;125:220–227.
4. Ciaglia P, Graniero KD. Percutaneous dilatational tracheostomy: results and long-term follow-up. *Chest* 1992;101:464–467.
5. Das P, Zhu H, Shah RK, Roberson DW, Berry J, Skinner ML. Tracheotomy-related catastrophic events: results of a national survey. *Laryngoscope* 2012;122:30–37.
6. Gilbey P. Fatal complications of percutaneous dilatational tracheostomy. *Am J Otolaryngol* 2012;33:770–773.
7. Shapiro M, Wilson RK, Casar G, Bloom K, Teague RB. Work of breathing through different sized endotracheal tubes. *Crit Care Med* 1986; 141028–1031.
8. Wright PE, Marini JJ, Bernard GR. In vitro versus in vivo comparison of endotracheal tube airflow resistance. *Am Rev Respir Dis* 1989;140:10–16.
9. Byron Mullins J, Templer JW, Davis WE, Kong J, Hinson J. Airway resistance and work of breathing in tracheostomy tubes. *Laryngoscope* 1993; 103:1367–1372.
10. Moorhouse J, Ali T, Moorhouse T, Owens D. Poorly placed tracheostomy tubes: effects on flow and resistance. *J Intensive Care Soc* 2015;16: 282–286.
11. Pryor LN, Baldwin CE, Ward EC, et al. Tracheostomy tube type and inner cannula selection impact pressure and resistance to air flow. *Respir Care* 2016; 61:607–614.
12. Yung MW, Snowdon SL. Respiratory resistance of tracheostomy tubes. *Arch Otolaryngol* 1984;110:591–595.
13. Davis K Jr, Campbell RS, Johannigman JA, Valente JF, Branson RD. Changes in respiratory mechanics after tracheostomy. *Arch Surg* 1999; 134:59–62.
14. Kleinstreuer C, Zhang Z, Li Z. Modeling airflow and particle transport/deposition in pulmonary airways. *Respir Physiol Neurobiol* 2008;163:128–138.
15. Worth Longest P, Vinchurkar S. Validating CFD predictions of respiratory aerosol deposition: effects of upstream transition and turbulence. *J Biomech* 2007;40:305–316.
16. Malve M, Perez del Palomar A, Chandra S, et al. FSI Analysis of a healthy and a stenotic human trachea under impedance-based boundary conditions. *J Biomech Eng* 2011;133:021001.
17. Mylavarapu G, Subramaniam D, Jonnagiri R, et al. Computational modeling of airway obstruction in sleep apnea in down syndrome: a feasibility study. *Otolaryngol Head Neck Surg* 2016;155:184–187.
18. Subramaniam DR, Mylavarapu G, Fleck RJ, Amin RS, Shott SR, Gutmark EJ. Effect of airflow and material models on tissue displacement for surgical planning of pharyngeal airways in pediatric down syndrome patients. *J Mech Behav Biomed Mater* 2017;71:122–135.
19. Sul B, Wallqvist A, Morris MJ, Reifman J, Rakesh V. A computational study of the respiratory airflow characteristics in normal and obstructed human airways. *Comput Biol Med* 2014;52:130–143.
20. Chowdhary R, Singh V, Tattersfield AE, Sharma SD, Kar S, Gupta AB. Relationship of flow and cross-sectional area to frictional stress in airway models of asthma. *J Asthma* 1999;36:419–426.
21. Epstein SK. Anatomy and physiology of tracheostomy. *Respir Care* 2005;50: 476–482.
22. Bates AJ, Cetto R, Doorly DJ, Schroter RC, Tolley NS, Comerford A. The effects of curvature and constriction on airflow and energy loss in pathological tracheas. *Respir Physiol Neurobiol* 2016;234:69–78.
23. Nikander K, Denyer J, Smith N, Wollmer P. Breathing patterns and aerosol delivery: impact of regular human patterns, and sine and square waveforms on rate of delivery. *J Aerosol Med* 2001;14:327–333.
24. Yang SC, Yang SP. Effects of inspiratory flow waveforms on lung mechanics, #gas |exchange, and respiratory metabolism in COPD patients during mechanical ventilation. *Chest* 2002;122:2096–2104.
25. Lin C-L, Tawhai MH, McLennan G, Hoffman EA. Characteristics of the turbulent laryngeal jet and its effect on airflow in the human intra-thoracic airways. *Respir Physiol Neurobiol* 2007;157:295–309.
26. Spiegel M, Redel T, Zhang YJ, et al. Tetrahedral vs. polyhedral mesh size evaluation on flow velocity and wall shear stress for cerebral hemodynamic simulation. *Comput Methods Biomech Biomed Engin* 2011;14:9–22.
27. Cebral JR, Summers RM. Tracheal and central bronchial aerodynamics using virtual bronchoscopy and computational fluid dynamics. *IEEE Trans Med Imaging* 2004;23:1021–1033.
28. Hess DR. Tracheostomy tubes and related appliances. *Respir Care* 2005;50: 497–510.
29. Ressler B, Lee RT, Randell SH, Drazen JM, Kamm RD. Molecular responses of rat tracheal epithelial cells to transmembrane pressure. *Am J Physiol Lung Cell Mol Physiol* 2000;278:L1264–L1272.
30. Gustin B, G'Sell C, Cochelin B, Wourms P, Potier-Ferry M. Finite element determination of the forces exerted by endotracheal tubes on the upper airways. *Biomaterials* 1996;17:1219–1225.
31. Pelosi P, Severgnini P. Tracheostomy must be individualized! *Crit Care* 2004;8:322–324.
32. Pandian V, Hutchinson CT, Schiavi AJ, et al. Predicting the need for nonstandard tracheostomy tubes in critically ill patients. *J Crit Care* 2017;37: 173–178.